Clinical Neurophysiology 130 (2019) 1596–1603

Contents lists available at ScienceDirect

Clinical Neurophysiology

journal homepage: www.elsevier.com/locate/clinph

Focal cortical dysplasia II-related seizures originate from the bottom of the dysplastic sulcus: A stereoelectroencephalography study

Wen-han Hu [a], Bao-tian Zhao [b], Chao Zhang [b], Xiu Wang [b], Lin Sang [c], Xiao-qiu Shao [d], Hui Qiao [a], Jian-guo Zhang [b], Kai Zhang [b,*]

[a] Beijing Neurosurgical Institute, Capital Medical University, Beijing, China
[b] Department of Neurosurgery, Beijing Tiantan Hospital, Capital Medical University, Beijing, China
[c] Department of Neurosurgery, Beijing Fengtai Hospital, Beijing, China
[d] Department of Neurology, Beijing Tiantan Hospital, Capital Medical University, Beijing, China

ARTICLE INFO

Article history:
Accepted 19 May 2019
Available online 22 June 2019

Keywords:
Epilepsy
Focal cortical dysplasia
Depth electrode
Stereoelectroencephalography
High-frequency oscillations

HIGHLIGHTS

- We explored the epileptogenic properties across the sulci with focal cortical dysplasia type II lesions using SEEG.
- Higher epileptogenicity index (EI) and more HFOs were recorded by bottom contacts than by non-bottom contacts.
- The EI value and HFO number were negatively correlated with distance from bottom.

ABSTRACT

Objectives: Focal cortical dysplasia (FCD) II is a frequently observed histopathological substrate in epilepsy surgery. In the present study, we explored the spatial distribution of epileptogenic activities across FCD II lesions using stereoelectroencephalography.

Methods: Patients with histopathologically confirmed type II FCDs and who had at least one depth electrode that go through the wall of the dysplastic sulcus from the surface to the bottom were included. The dysplastic sulci were divided into the bottom and non-bottom parts manually, and contacts were defined as bottom or non-bottom contacts according to their locations. Factors (bottom location, pathological subtype, magnetic resonance imaging manifestation, and presence of bottom-of-sulcus dysplasia) potentially associated with earliest onset identified by conventional visual analysis, epileptogenicity index (EI), and standardized number of high-frequency oscillations (HFOs) were analyzed. Linear regression analyses between distance (from the location of the analyzed contact to the bottom of the sulcus) and EI value and HFO number were performed.

Results: Sixteen patients with 19 depth electrodes containing 112 valid contacts were included. Bottom location was the sole factor significantly associated with earliest onset ($P < 0.001$), EI value ($P < 0.001$), and HFO number ($P < 0.001$). Most earliest onsets were recorded by the bottom contacts, bottom contacts had higher EI value (0.81 ± 0.28 vs. 0.31 ± 0.24, $P < 0.001$) and more HFOs (0.78 ± 0.28 vs. 0.35 ± 0.31, $P < 0.001$) than non-bottom contacts. Moreover, the EI value ($R = -0.72$, $P < 0.001$) and HFO number ($R = -0.64$, $P < 0.001$) were significantly negatively correlated with distance, regardless of histopathological subtype, MRI manifestation, or absence of bottom-of-sulcus dysplasia.

Conclusion: Seizure onsets and interictal HFOs most often arise from the bottom part of a sulcus with type II FCD.

Significance: The findings of the present study contribute to intracranial electrode selection, trajectory planning, and, later on, resection of this kind of malformation.

© 2019 International Federation of Clinical Neurophysiology. Published by Elsevier B.V. All rights reserved.

* Corresponding author.
E-mail address: zhangkai62035@163.com (K. Zhang).

https://doi.org/10.1016/j.clinph.2019.05.029
1388-2457/© 2019 International Federation of Clinical Neurophysiology. Published by Elsevier B.V. All rights reserved.

1. Introduction

Focal cortical dysplasia (FCD) II, a specific malformation characterized by dysmorphic neurons with or without balloon cells histopathologically, was first described by Taylor et al. (1971). It is a surgically remediable substrate with favorable postoperative seizure outcomes accounting for 9% of all patients who undergo epilepsy surgery, with a higher proportion (17%) in the pediatric population (Blumcke et al., 2017). A number of reports demonstrated that the rate of becoming seizure-free was up to approximately 80% (Chassoux et al., 2010, Tassi et al., 2002, Urbach et al., 2002, Wagner et al., 2011), and patients with magnetic resonance imaging (MRI)-visible or type IIB FCD lesions tend to have complete resection, thus resulting in more favorable seizure outcomes compared to those with MRI-invisible or type IIA lesions (Lerner et al., 2009, Tassi et al., 2012).

Several characteristics of this kind of epileptogenic brain malformation have been summarized in previous studies. It was reported that patients with FCD II are more likely to have the first onset in childhood, that the seizures are frequent and stereotyped, and that the lesions are predominantly extratemporally located (Chassoux et al., 2012). Neuroimaging studies demonstrated that gray-white matter junction blurring, cortical hyperintensity in T2 or fluid-attenuated inversion recovery (FLAIR) sequences, abnormal gyration/sulcation, cortical thickening, and "transmantle sign" are typical MRI features of FCD II (Colombo et al., 2012, Krsek et al., 2008, Krsek et al., 2009, Liu et al., 2019). A specific electrographic pattern, characterized by rhythmic or pseudo-rhythmic spikes and polyspikes, can be frequently recorded during scalp electroencephalographic (EEG) monitoring (Tassi et al., 2012). Similar to scalp EEG studies, intracranial electrophysiological studies also revealed biomarkers, including repetitive subcontinuous spikes, spikes and waves, polyspikes, or bursts of fast rhythms, in this specific malformation (Guerrini et al., 2015).

Some neuroimaging studies demonstrated that FCD II lesions tend to be bottom of sulcus located (Besson et al., 2008, Harvey et al., 2015). Previous reports revealed the value of stereoelectroencephalography (SEEG) in detecting FCD (Chassoux, 2003, McGonigal et al., 2007), while the spatial distribution of electrophysiological abnormalities and the site of seizure origination across the FCD II lesions remain unexplored in those studies.

In this study, conventional visual analyses and quantitative methods were used to explore the epileptogenic properties across FCD II lesions detected by depth electrodes in patients under stereoelectroencephalography (SEEG) monitoring. The quantification was performed by calculating the epileptogenicity index (EI) and counting interictal high-frequency oscillations (HFOs). We suppose that the bottom part of the dysplastic sulcus presents the most intense epileptogenicity. Depth electrodes that went through one wall of the dysplastic sulcus from the surface to the bottom were included. For each selected contact, the relationship between quantified epileptogenic properties (EI value and HFO number) and their distance to the bottom of the sulcus was analyzed.

2. Methods

2.1. Patient selection

Consecutive patients who underwent resective epilepsy surgery at the Beijing Tiantan-fengtai Epilepsy Center from January 2015 to December 2017 were retrospectively included using the following criteria: (1) the patients underwent SEEG monitoring before resective surgery, (2) at least one depth electrode that went through one wall of the dysplastic sulcus confirmed by MRI, positron emission tomography (PET)/MRI coregistration, or SEEG recordings from the surface to the bottom, (3) tailored focal corticectomies were performed, and the histopathological diagnoses were FCD II, which was defined as abnormal cortical lamination with dysmorphic neurons alone (IIA) or together with balloon cells (IIB) according to the 2011 International League Against Epilepsy (ILAE) FCD classification system (Blumcke et al., 2011). Before depth electrode implantation, a comprehensive pre-surgical evaluation, including clinical history, neurological examination, scalp EEG monitoring, routine MRI, ^{18}F-fluorodeoxyglucose (FDG)-PET and image post-processing, was performed for all the patients.

This research was approved by the institutional review board of the Beijing Tiantan Hospital, and informed consent was obtained from all included participants.

2.2. Electrode placement and SEEG recording

Intracerebral multiple contact electrodes (Huake-Hengsheng Medical Technology, Beijing, China; 8–16 contacts, length: 2 mm, diameter: 0.8 mm, 1.5 mm apart) were placed using a CRW frame-based system (Integra Radionics, Burlington, MA, USA) to record intracranial EEG data. The strategy of electrode placement, independent from the present study, was based on above-mentioned non-invasive information providing clinical hypotheses about the localization of the epileptogenic zone (EZ). A postoperative computerized tomography (CT) scan was performed to confirm the absence of intracranial bleeding and the accuracy of electrode position. Twenty-four hours after electrode implantation, electrophysiological signals were recorded on a video EEG system (Nihon-Kohden, Tokyo, Japan) with a sampling rate of 1000 Hz or 2000 Hz. Long-term SEEG monitoring was carried out to record at least two habitual seizures.

2.3. Electrode and contact selection

For MRI-positive lesions, the dysplastic sulci were localized by a conventional visual analysis and morphometric analysis program (Hu et al., 2018, Wang et al., 2015). For MRI-negative lesions, the sulci showed focal hypometabolism with PET/MRI fusion, and the earliest seizure onset pattern during SEEG monitoring was identified (Chassoux et al., 2010). The 3D-T1 MRI and post-implantation CT images were imported into the IntrAnat Electrodes software (Grenoble Institut des Neurosciences, Grenoble, France; https://f-tract.eu/software/intranat), and the electrodes were manually labeled and positioned (Deman et al., 2018). The electrode was positioned by choosing a corresponding model and clicking on the post-implantation images at the end of the electrode and any other point along its trajectory. Electrodes with trajectories that went through the wall of dysplastic sulcus from the surface to the bottom were selected for analyses. Based on the 3D-T1 MRI image, we drew a line intersecting the bottom point of the sulcus and parallel to the tangent to the interior border of the gray matter. This line divided the dysplastic sulcus into bottom and non-bottom parts. For the included electrodes, contacts outside the brain or totally in the white matter were excluded. Contacts partially or totally in the bottom part were identified as "bottom" contacts, and the others were identified as "non-bottom" contacts (Fig. 1).

2.4. Visual analysis of ictal data

At the beginning of visual analysis, the SEEG signals were re-referenced with a contact in white matter tissue as the common reference contact for all channels. Since the bottom contacts of each selected electrode were always labeled by smaller numbers and the corresponding channels were arranged in the upper part of the channel group, the sequence of channels was randomized

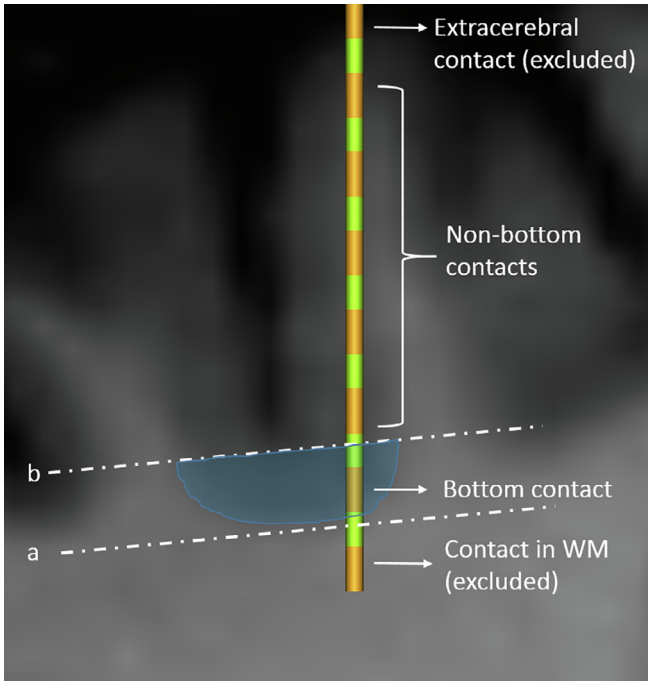

Fig. 1. Schematic diagram of the divisions of a sulcus and labeling of contacts. Line a is tangential to the interior border of the gray matter in the sulcus bottom and line b is parallel to line a, intersecting the bottom point of the sulcus. Brain tissue interior and exterior to line b are defined as bottom and non-bottom parts, respectively. Contacts partially outside brain tissue or completely in white matter were labeled as extracerebral and white-matter contacts, respectively, and excluded from analyses. For the remaining contacts, if they were partially or totally in the bottom part, they were identified as bottom contacts. Otherwise, they were identified as non-bottom contacts. WM: white matter.

to avoid bias during visual analysis. Two habitual seizures were randomly selected and visually analyzed by two epileptologists blinded to the channel labels, and time-frequency spectrograms were also provided for assistance (Fig. 2). Channels with the earliest seizure onset pattern in each electrode were marked, and any discrepancies were resolved through discussion.

2.5. Quantitative analysis of ictal data: EI calculation

EI was calculated for two habitual seizures for each electrode by a plug-in implanted in the Anywave software (INSERM, Marseille, France; http://meg.univ-amu.fr) (Colombet et al., 2015). The EI was used to quantify the epileptogenicity of cerebral structures and described in detail in a previous study (Bartolomei et al., 2008). In brief, the EI is a normalized quantity ranging from 0 (no epileptogenicity) to 1 (maximal epileptogenicity). Two factors were taken into account when computing the EI: the first one is the generation of a fast discharge estimated by signal energy ratio (ER) between high (beta [12–24 Hz], gamma [24–127 Hz]) and low (theta [4–7.4 Hz] and alpha [7.4–12 Hz]) frequency bands, and the second one is change-points in the ER[n] quantity estimated with a designed threshold. The EI allows quantitative estimation of the combination of these two phenomena and can be used as a classification measure. Contacts involved in seizure onset detected by EI were further validated by visual analysis. EI values from all included contacts were computed and averaged for 2 habitual seizures in each patient.

2.6. Analysis of interictal data

Since sleep SEEG recording clips have fewer movement artifacts and include more interictal discharges, 5-minute sleep recording clips were selected randomly for analysis of all patients. Interictal HFOs were automatically detected using an inhouse MATLAB R2013a (MathWorks, MA, USA) script and validated manually by an epileptologist blinded to the channel label. For semi-automatic detection, in general, raw data of multichannel SEEG segments were first filtered using a 3-order Butterworth digital band-pass filter in the 80–500 Hz range using the filtfilt function in MATLAB. Then, the standard deviations (SDs) of the band-pass filtered signal in 100 ms windows were calculated, and the amplitude threshold was set to 5 times the median of the SDs. For all samples with amplitudes larger than the threshold, an epoch of 100 ms before and after the sample were extracted from the raw data as candidates. The candidate epochs were then transformed into scalograms through wavelet transform for manual validation and classification. To validate the reliability of the proposed

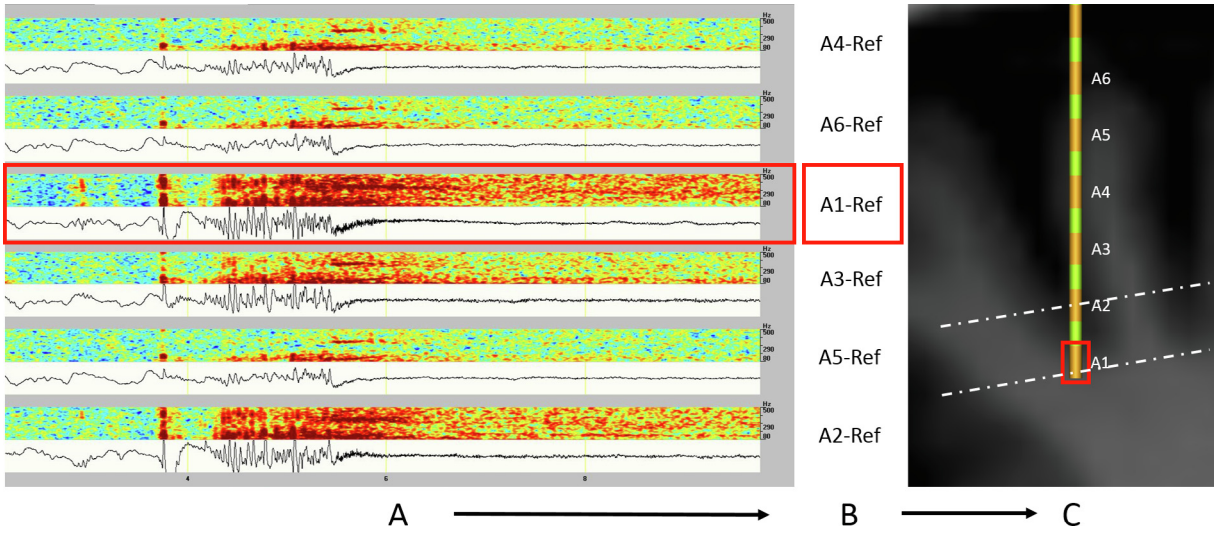

Fig. 2. Workflow of visual analysis of ictal data. (A) The raw SEEG signals of ictal epochs and corresponding time-frequency spectrograms were provided for visual analysis. Please note that label information was hidden and the sequence of channels in each electrode was randomized to avoid a bias. (B) Label information for each contact. (C) Location of each contact according to the label information. The onset channel, label and contact were marked by a red box. SEEG: stereoelectroencephalography.

semi-automatic detection procedure, we compared the HFO counts from 4 subjects of this cohort (patient 2, 5, 8 and 9) between the semi-automatic detection method and full visual analysis before final analysis. The number of detected HFOs in each contact was normalized by dividing the maximal number from the same electrode.

2.7. Distance calculation

The distance from each included contact to the bottom of the dysplastic sulcus was calculated according to the three-dimensional coordinates of the 3D-T1 MRI image. The coordinates of contacts and bottom points of dysplastic sulci were derived from IntrAnat Electrodes and Statistical Parametric Mapping (SPM) version 8 (Wellcome Trust Centre for Neuroimaging, London, UK; http://www.fil.ion.ucl.ac.uk/spm), respectively. For each contact, the distances to all bottom points of the corresponding sulcus were calculated, and the minimal one was selected for subsequent analyses. Moreover, the distances of all bottom contacts were set as zero. Similar to EI value and HFO number, the distance was normalized by dividing the maximal value at the same electrode.

2.8. Statistical analysis

To identify potential factors including bottom location, pathological subtype, MRI manifestation, or presence of bottom-of-sulcus dysplasia (BOSD) associated with earliest seizure onset by visually analysis, and EI value or HFO number by quantitative analysis of each included contact, binary logistic regression and multiway ANOVA was performed respectively. To explore the correlation between the distance from bottom and the epileptogenicity, we performed linear regression analysis between distance and EI value and HFO number. We further divided FCD lesions into IIA and IIB, MRI-positive (MRI+) and -negative (MRI−), or BOSD and non-BOSD subgroups, and comparisons and linear regression analyses were also performed within the subgroups. The independent t test (two-tailed) was performed for comparisons of independent numerical data if the variables were normally distributed. Otherwise, Mann-Whitney U-tests were used. Pearson correlation analysis was used to evaluate the relationship between distance and epileptogenicity (EI value and HFO number). Significance was defined as $P \leq 0.05$. The statistical tests were performed with R version 3.5.0 software (R Foundation for Statistical Computing, Vienna, Austria; http://www.R-project.org).

3. Results

3.1. Patient demographics and clinical information

Sixteen (7 female and 9 male) refractory epilepsy patients with histologically proven FCD II and a proper electrode implantation pattern were included. The mean age at surgery was 16.50 ± 8.41 years, and the mean epilepsy duration was 8.28 ± 6.58 years. The FCD lesions were located in the frontal lobe in 13 patients, and parietal, temporal, and frontoparietal lobe in one patient each. Five lesions were visible on MRI scanning, two were diagnosed as BOSD, and 10 were histopathologically proven subtype IIA. According to Engel's scale, 13 patients were strictly seizure-free (Engel Ia) at the last follow-up (Table 1).

3.2. Electrode information

Three patients had 2 electrodes included in this study. In total, there were 19 electrodes with 112 contacts for analysis. Among the 112 contacts, 32 were partially or totally located in the bottom part of the dysplastic sulci.

3.3. Results of visual analysis

Two ictal epochs were selected for each electrode, which led to 224 channels (64 bottom channels and 160 non-bottom channels) including 38 (19 electrodes with two ictal epochs) earliest onset epochs in total. Among the 38 onsets, 37 and one were recorded by bottom and non-bottom contacts, respectively. Thirty-seven of 64 (57.81%) bottom channels showed earliest onsets and only one of 160 (0.63%) non-bottom channels showed earliest onset, and binary logistic regression indicated only bottom location was strongly associated with earliest onset (bottom location, $P < 0.001$; MRI manifestation, $P = 0.571$; pathological subtype, $P = 0.100$; presence of BOSD, $P = 0.882$).

Table 1
Patient demographics and clinical information.

Patient	Sex*	Age at surgery (y)	Epilepsy duration (y)	FCD location	SZ semiology	Interictal scalp EEG	Ictal scalp EEG	MRI#	BOSD	Electrode placement	Pathology	Outcome	Follow-up (y)
1	M	22	13	L F	Motor	L FC	L FC	P	No	L FP	IIB	II	4
2	M	25	17	L F	Motor	L C	Non-lat	N	No	L FP	IIA	Id	3
3	M	5	1	R T	Dialeptic SZ	R T	R FT	N	No	R T	IIA	Ia	3
4	M	12	4	R F	BATS	R FC	R FC	N	No	R F	IIA	Ia	4
5	M	16	1.5	R F	Dialeptic SZ	B F	R F	N	No	R FT	IIA	Ia	3
6	F	19	10	L F	Hypermotor	B FT	L FT	N	No	L FIP	IIA	Ia	3
7	M	6	3	R F	Fear	B FC	Non-lat	N	No	R FP	IIA	Ia	4
8	F	24	7	R F	Version	R FC	R FC	N	No	R FP	IIA	Ia	3
9	F	14	9	R F	Version	R FC	R F	N	No	R FTI	IIB	Ia	2
10	F	10	4	R F	Fear, dystonia	R F	L F	N	No	R F	IIB	Ia	2
11	M	36	23	R F	Hypermotor	Non-lat	Non-lat	P	Yes	R FI	IIB	Ib	4
12	F	11	6	L FP	Motor	L FCP	L H	P	No	L FPI	IIB	Ia	2
13	F	17	12	L F	Version	L FT	L FC	P	No	L FT	IIA	Ia	4
14	F	26	17	R P	Dystonia	R CP	R CP	P	Yes	R FTP	IIB	Ia	2
15	M	8	1	L F	Dialeptic SZ	L FT	L FT	N	No	L F	IIA	Ia	4
16	M	13	4	L F	Dystonia	L FCP	L H	N	No	L FP	IIA	Ia	1

B: bilateral; BATS: bilateral asymmetric tonic seizure; C: central.
* F: female; F: frontal; H: hemispheric; I: insular; L: left; N: negative; Non-lat, non-lateralized.
# P: positive; P: parietal; R: right; SEEG: stereoelectroencephalography; SZ: seizure; T: temporal.

3.4. Results of EI analysis

In general, a multi-way ANOVA showed that bottom location was the sole factor influencing the EI value (bottom location, $P < 0.001$; pathological subtype, $P = 0.720$; MRI manifestation, $P = 0.571$; presence of BOSD, $P = 0.450$), and the bottom contacts had higher value than the non-bottom ones (0.81 ± 0.28 vs. 0.31 ± 0.24, $P < 0.001$) (Fig. 3A). Furthermore, regression analysis revealed a significant negative correlation between EI value and distance (all: $R = -0.72$, $P < 0.001$; IIA: $R = -0.71$, $P < 0.001$; IIB: $R = -0.76$, $P < 0.001$; MRI+: $R = -0.82$, $P < 0.001$; MRI−: $R = -0.70$, $P < 0.001$; BOSD: $R = -0.94$, $P < 0.001$; non-BOSD: $R = -0.67$, $P < 0.001$) (Fig. 3B–E).

3.5. Results of HFO analysis

Firstly, the reliability of the semi-automatic HFO detection method was validated from 4 patients and the overall sensitivity and specificity were 83.5% and 96.8% respectively compared with full visual analysis. Similar to EI analysis, only bottom location had a significant association with HFO number (bottom location, $P < 0.001$; pathological subtype, $P = 0.657$; MRI manifestation, $P = 0.386$; presence of BOSD, $P = 0.669$), and more HFOs were detected in the bottom parts of dysplastic sulci than in the non-bottom parts (0.78 ± 0.28 vs. 0.35 ± 0.31, $P < 0.001$) (Fig. 4A). Our data also demonstrated a strong negative correlation between HFO number and distance (all: $R = -0.64$, $P < 0.001$; IIA: $R = -0.59$, $P < 0.001$; IIB: $R = -0.75$, $P < 0.001$; MRI+: $R = -0.66$, $P < 0.001$; MRI−: $R = -0.62$, $P < 0.001$; BOSD: $R = -0.92$, $P < 0.001$; non-BOSD: $R = -0.60$, $P < 0.001$) (Fig. 4B–E).

4. Discussion

Knowledge of the spatial distribution of FCD II-related epileptic discharges and seizure onset can contribute to intracranial electrode selection, trajectory planning, and, later on, lesion resection. The present study demonstrated that interictal HFOs predominate at the bottom of the dysplastic sulcus. For ictal data, visual and quantitative analyses also indicated that most seizures originated from the bottom of the dysplastic sulcus. Moreover, linear regres-

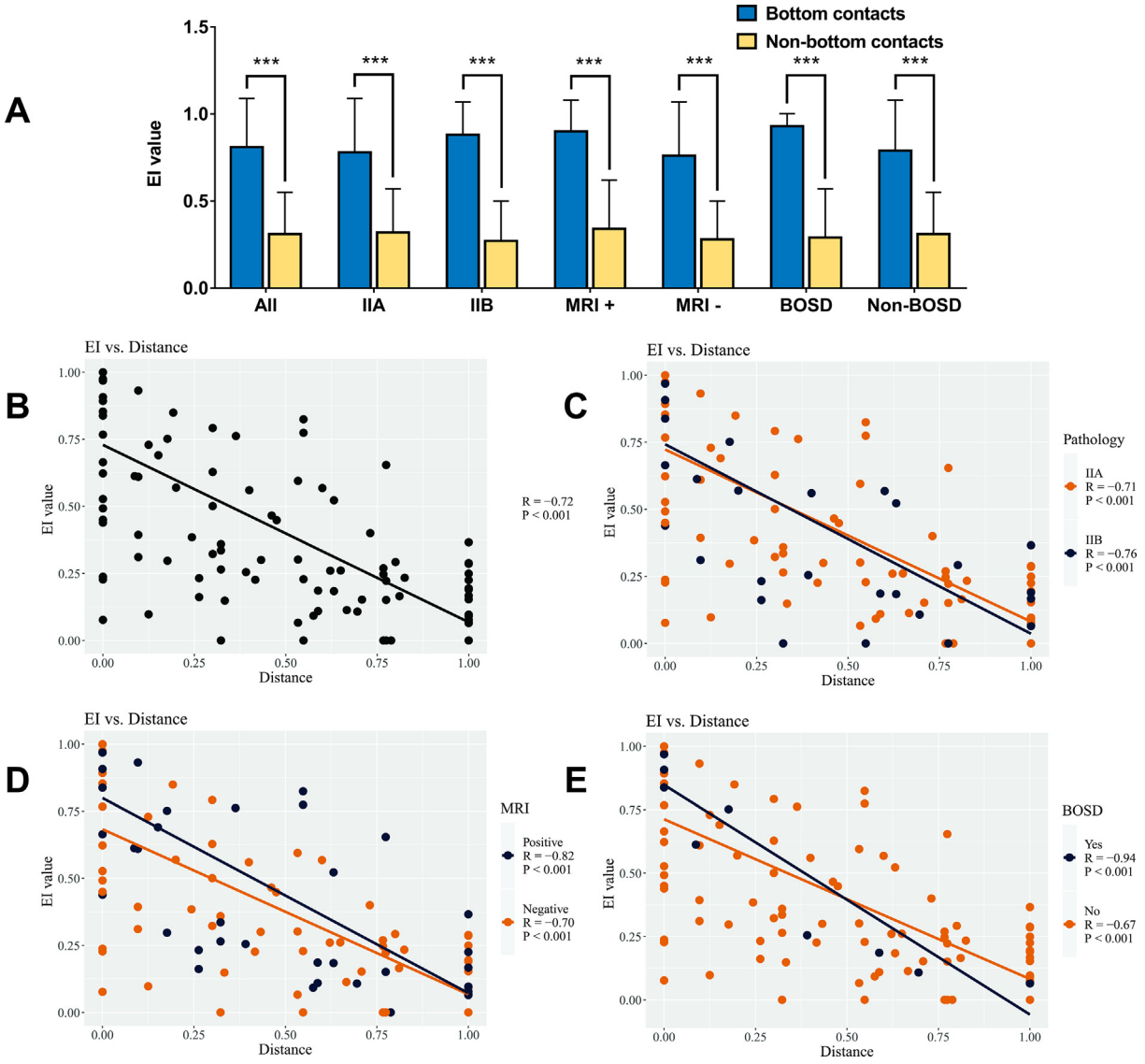

Fig. 3. Quantitative analyses of ictal data. (A) Comparisons of EI between bottom and non-bottom groups. EI value correlates directly with distance from contact to the bottom of the dysplastic sulcus (B), regardless of histopathological subtype (C), MRI manifestation (D), or absence of BOSD (E). Please note some dots are overlapped. BOSD: bottom-of-sulcus dysplasia; EI: epileptogenicity index.

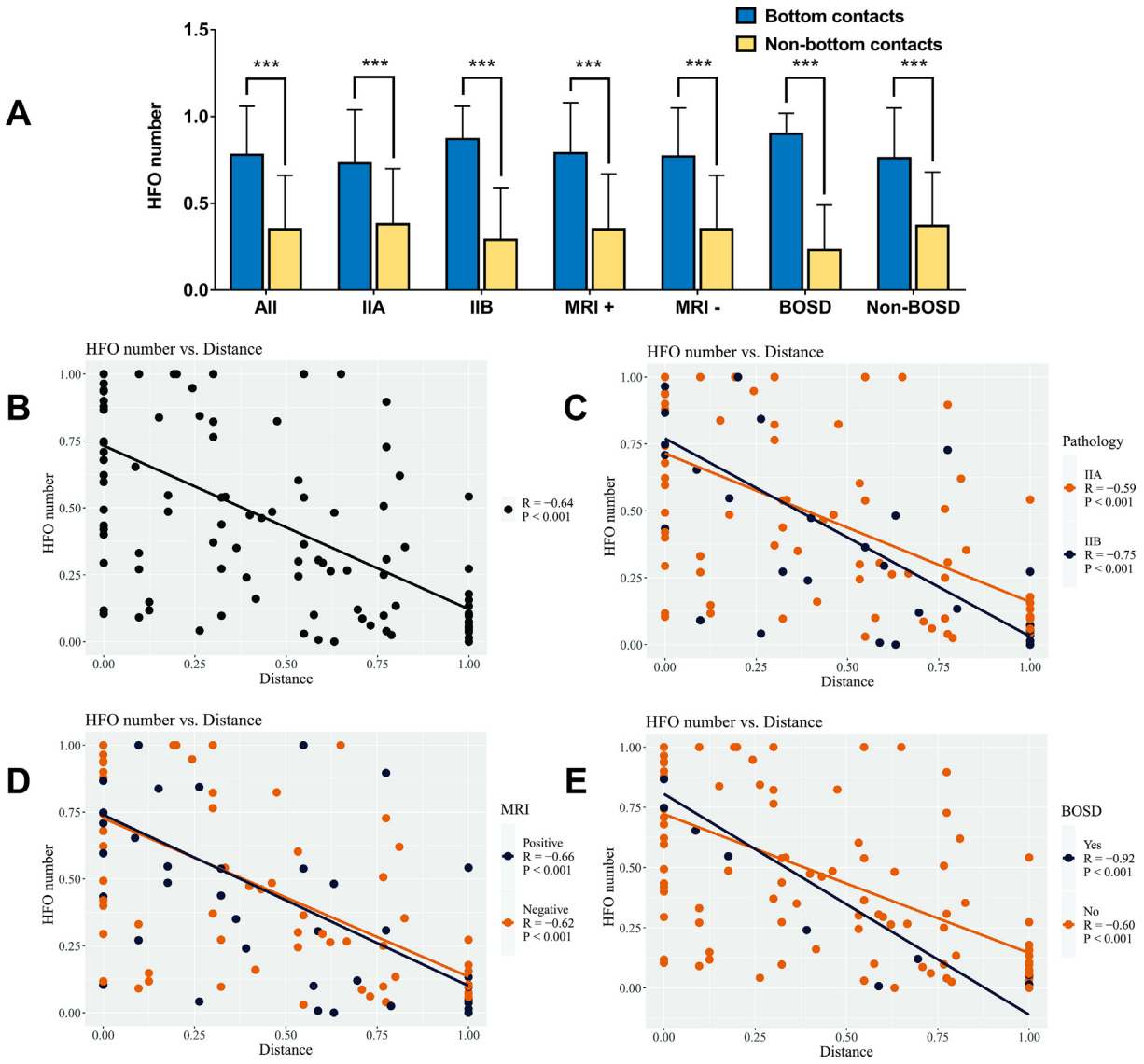

Fig. 4. Analyses of interictal HFO number. (A) Comparisons of HFO number between bottom and non-bottom groups. HFO number is significantly negatively correlated with distance (B), regardless of histopathological subtype (C), MRI manifestation (D), or absence of BOSD (E). Please note some dots are overlapped. BOSD: bottom-of-sulcus dysplasia, HFO: high-frequency oscillation.

sion analyses demonstrated that the EI value and HFO number were significantly negatively correlated with the distance from the bottom, regardless of histopathological subtype, MRI manifestation, or absence of BOSD.

It is well known that the EZ where seizures initiate also generates interictal epileptiform spikes and sharp waves (Gloor, 1975). These interictal EEG patterns represent the paroxysmal discharge of large neuronal populations that are highly specific to epilepsy (Ayala et al., 1973). However, the significance of spikes in defining the EZ remains controversial. In addition to the EZ, spikes can be seen in other brain areas outside the EZ. Therefore, spikes are widely accepted to define the irritative zone (IZ) instead of the EZ (Rosenow and Luders, 2001). It is unclear how this abnormal electrophysiological activity is related to epileptogenesis (Hufnagel et al., 2000, Rosenow and Luders, 2001). Interictal HFOs, with frequency ranging from 80 to 500 Hz, were first recorded in the human brain by Bragin et al. (1999). Since then, it has been frequently reported that HFOs are an interictal signature of epileptogenic networks involved in seizure generation and even epileptogenesis (Worrell and Gotman, 2011), and HFOs represent a marker for EZ independent of the underlying pathology (Jacobs et al., 2009). However, the specificity of interictal HFOs in defining the EZ remains undetermined because it is not clear how to separate pathological HFOs from normal physiological oscillations (Engel et al., 2009, Le Van Quyen et al., 2006). A recent study suggested that HFOs are not a better biomarker of epileptogenic tissue than spikes (Roehri et al., 2018). Moreover, removal cerebral tissue generating HFOs is not necessary for seizure freedom, which suggests HFOs may be less specific for epileptic tissue than earlier studies have indicated (Jacobs et al., 2018). In summary, although HFOs are not the perfect interictal biomarker of epilepsy, they are the most practical signature to date. With respect to ictal epochs, intracranial EEG studies showed that partial seizures often begin with low-amplitude HFOs (Lagarde et al., 2016, Perucca et al., 2014), and better postsurgical outcomes are associated with this kind of onset pattern (Lagarde et al., 2016). EI proposed by Bartolomei et al. mixed the spectral and temporal information of each electrode to quantify the epileptogenicity of cerebral structures

(Bartolomei et al., 2008). With this quantitative method, we can analyze the relationship between epileptogenicity and distance from the bottom.

Besson et al. explored the spatial relationship between FCD lesions and brain sulci using automated sulcal extraction and morphometry, and a conclusion was made that small FCDs were located at the bottom of a deep sulcus (Besson et al., 2008). Our data were consistent with this neuroimaging study: interictal epileptic activities predominated at the bottom of dysplastic sulcus, and most seizures originated from it. In addition to small FCDs, the present study included patients with MRI-negative and large (MRI abnormalities extending from the bottom to the wall or crown) FCDs. For MRI-negative lesions, it is impossible to analyze them by MRI techniques. All FCDs labeled as MRI negative in the present study were strictly invisible on MRI since they were undetectable even with sophisticated image post-processing techniques. Nevertheless, SEEG gives us the opportunity to explore the spatial distribution of the epileptogenic activities and the site of seizure origination across the FCD lesions. We postulated the MRI-negative lesions were too subtle to be visible, and previous study indicated subtle FCDs were located at the bottom (Besson et al., 2008). It is not surprising that epileptic activities predominated at the bottom in MRI-negative cases. What is interesting is that although MRI abnormalities were observed through the whole sulci in some cases, seizures also originated from the bottom. Our former study still indicated that MRI abnormalities predominated in the bottom part of the sulcus in those cases (Liu et al., 2019). Further studies should explore the correlation between MRI abnormalities and epileptogenicity, furthermore, which components of this kind of malformation are responsible for epileptic discharges or onset.

Subdural EEG (SDEEG) was widely used in the phase 2 evaluation for complicated epilepsy surgery cases, it has some advantages including large cortical coverage for delineating the extent of surgical margin or eloquent cortex, convenience in functional mapping, and feasibility for young children and infants compared to SEEG. On the other hand, this method has disadvantages including weakness for bilateral epilepsy or deep-seated epileptogenic foci, inadequate time for interpretation before surgery, and impracticability of radiofrequency thermocoagulation (Iida and Otsubo, 2017). The present study also demonstrated the disadvantage of SDEEG in exploring FCD II. Taking the most superficial contact of each depth electrode as a contact of subdural electrode placed on the surface of brain, fewer interictal epileptic discharges or tonic onsets were recorded compared to those deeper contacts. From this aspect, SEEG is preferred in detection of type II FCDs during the phase 2 evaluation.

The method and technique of SEEG were developed by Jean Talairach and Jean Bancaud during the 1950s (Bancaud et al., 1970); orthogonal electrode implantation using the Talairach stereotactic frame and the double grid system has been the classic and most established approach (Talairach et al., 1992). Orthogonal trajectories facilitate accurate implantation and subsequent interpretation of the electrode positions. Therefore, although it has entered the era of robots without Talairach stereotactic frame, orthogonal fashion is still widely used (Gonzalez-Martinez et al., 2016). However, the volume of the bottom part of a sulcus is much smaller than that of the non-bottom part, an orthogonal trajectory without bottom-aimed planning might easily miss the sulcus bottom. Therefore, for type II FCDs, we strongly recommend the trajectory of the depth electrode should run through the inferior portion of the dysplastic sulcus.

The present study also provided neuroelectrophysiological evidence for resective planning of FCD II. Since epileptic activities and seizure onsets are predominately recorded in the bottom part, complete removal of the bottom cortex is crucial for favorable post-operative seizure outcome. However, complete resection is sometimes difficult, especially when there are rich vessels at the bottom. Taking insular FCD as an example, the trunks of middle cerebral artery lie at the bottom of insular sulci, and the branches arising from those trunks supply the corresponding sulci and gyri. The neurosurgeon should cut off the suppling branches and lift the trunks in order to reach the bottom.

The first limitation of the current study is the small patient sample size, which produces relatively weak statistical power and limited generalizability. There may be two reasons for this limitation. The first one is that some locations of FCD lesions make it difficult to implant electrodes in the fashion that we proposed. The locations include cingulate, orbitofrontal, and insular areas. Another reason is the negative histopathological findings due to fragmentation of specimens, although electroclinical (repetitive subcontinuous spikes, spike-and-waves, polyspikes, or bursts of fast rhythms) or neuroimaging (gray-white matter junction blurring, cortical FLAIR hyperintensity, or transmantle sign) data highly indicated type II FCDs. The second limitation is that we could not explore the relationship between complete resection of bottom part of dysplastic sulcus with postsurgical seizure outcome, since only two patients had incomplete resection of FCD lesions due to eloquent cortex. The third limitation is about the value of HFOs in defining epileptogenicity and the method of HFO detection. As we previous mentioned, although HFOs have been proposed as a promising biomarker in many studies, their clinical value is still under evaluation. As for the quantified analysis of HFOs, visual analysis of large dataset was laborious and time consuming, and the performance of different automatic detectors varied. Many detectors performed well when validated against visual marking, however, the lack of robustness decreased their clinical value. To balance between convenience and robustness of HFO detection, in this study, we adopted and validated a semi-automatic detection approach to quantify the HFO counts.

Acknowledgments

This work is partly sponsored by Grants from the Capital (China) Health Research and Development Special Fund (2016-1-1071), the Beijing Municipal Science & Technology Commission (Z161100000216130 and Z171100001017069), and National Natural Science Foundation of China (No. 81771399, 81641053, 81701276).

Declaration of Competing Interest

None of the authors have any conflicts of interest to disclose.

References

Ayala GF, Dichter M, Gumnit RJ, Matsumoto H, Spencer WA. Genesis of epileptic interictal spikes. New knowledge of cortical feedback systems suggests a neurophysiological explanation of brief paroxysms. Brain Res 1973;52:1–17.

Bancaud J, Angelergues R, Bernouilli C, Bonis A, Bordas-Ferrer M, Bresson M, et al. Functional stereotaxic exploration (SEEG) of epilepsy. Electroencephalogr Clin Neurophysiol 1970;28:85–6.

Bartolomei F, Chauvel P, Wendling F. Epileptogenicity of brain structures in human temporal lobe epilepsy: a quantified study from intracerebral EEG. Brain 2008;131:1818–30.

Besson P, Andermann F, Dubeau F, Bernasconi A. Small focal cortical dysplasia lesions are located at the bottom of a deep sulcus. Brain 2008;131:3246–55.

Blumcke I, Spreafico R, Haaker G, Coras R, Kobow K, Bien CG, et al. Histopathological findings in brain tissue obtained during epilepsy surgery. New Engl J Med 2017;377:1648–56.

Blumcke I, Thom M, Aronica E, Armstrong DD, Vinters HV, Palmini A, et al. The clinicopathologic spectrum of focal cortical dysplasias: a consensus classification proposed by an ad hoc Task Force of the ILAE Diagnostic Methods Commission. Epilepsia 2011;52:158–74.

Bragin A, Engel Jr J, Wilson CL, Fried I, Buzsaki G. High-frequency oscillations in human brain. Hippocampus 1999;9:137–42.

Chassoux F. Stereo-EEG: the Sainte-Anne experience in focal cortical dysplasias. Epileptic Disord 2003;5(Suppl 2):S95–S103.
Chassoux F, Landre E, Mellerio C, Turak B, Mann MW, Daumas-Duport C, et al. Type II focal cortical dysplasia: electroclinical phenotype and surgical outcome related to imaging. Epilepsia 2012;53:349–58.
Chassoux F, Rodrigo S, Semah F, Beuvon F, Landre E, Devaux B, et al. FDG-PET improves surgical outcome in negative MRI Taylor-type focal cortical dysplasias. Neurology 2010;75:2168–75.
Colombet B, Woodman M, Badier JM, Benar CG. AnyWave: a cross-platform and modular software for visualizing and processing electrophysiological signals. J Neurosci Methods 2015;242:118–26.
Colombo N, Tassi L, Deleo F, Citterio A, Bramerio M, Mai R, et al. Focal cortical dysplasia type IIa and IIb: MRI aspects in 118 cases proven by histopathology. Neuroradiology 2012;54:1065–77.
Deman P, Bhattacharjee M, Tadel F, Job AS, Riviere D, Cointepas Y, et al. IntrAnat electrodes: a free database and visualization software for intracranial electroencephalographic data processed for case and group studies. Front Neuroinform 2018;12:40.
Engel Jr J, Bragin A, Staba R, Mody I. High-frequency oscillations: what is normal and what is not? Epilepsia 2009;50:598–604.
Gloor P. Contributions of electroencephalography and electrocorticography to the neurosurgical treatment of the epilepsies. Adv Neurol 1975;8:59–105.
Gonzalez-Martinez J, Bulacio J, Thompson S, Gale J, Smithason S, Najm I, et al. Technique, results, and complications related to robot-assisted stereoelectroencephalography. Neurosurgery 2016;78:169–80.
Guerrini R, Duchowny M, Jayakar P, Krsek P, Kahane P, Tassi L, et al. Diagnostic methods and treatment options for focal cortical dysplasia. Epilepsia 2015;56:1669–86.
Harvey AS, Mandelstam SA, Maixner WJ, Leventer RJ, Semmelroch M, MacGregor D, et al. The surgically remediable syndrome of epilepsy associated with bottom-of-sulcus dysplasia. Neurology 2015;84:2021–8.
Hu WH, Wang X, Liu LN, Shao XQ, Zhang K, Ma YS, et al. Multimodality image post-processing in detection of extratemporal MRI-negative cortical dysplasia. Front Neurol 2018;9:450.
Hufnagel A, Dumpelmann M, Zentner J, Schijns O, Elger CE. Clinical relevance of quantified intracranial interictal spike activity in presurgical evaluation of epilepsy. Epilepsia 2000;41:467–78.
Iida K, Otsubo H. Stereoelectroencephalography: Indication and Efficacy. Neurol Med Chir (Tokyo) 2017;57:375–85.
Jacobs J, Levan P, Chatillon CE, Olivier A, Dubeau F, Gotman J. High frequency oscillations in intracranial EEGs mark epileptogenicity rather than lesion type. Brain 2009;132:1022–37.
Jacobs J, Wu JY, Perucca P, Zelmann R, Mader M, Dubeau F, et al. Removing high-frequency oscillations: a prospective multicenter study on seizure outcome. Neurology 2018;91:e1040–52.
Krsek P, Maton B, Korman B, Pacheco-Jacome E, Jayakar P, Dunoyer C, et al. Different features of histopathological subtypes of pediatric focal cortical dysplasia. Ann Neurol 2008;63:758–69.
Krsek P, Pieper T, Karlmeier A, Hildebrandt M, Kolodziejczyk D, Winkler P, et al. Different presurgical characteristics and seizure outcomes in children with focal cortical dysplasia type I or II. Epilepsia 2009;50:125–37.
Lagarde S, Bonini F, McGonigal A, Chauvel P, Gavaret M, Scavarda D, et al. Seizure-onset patterns in focal cortical dysplasia and neurodevelopmental tumors: relationship with surgical prognosis and neuropathologic subtypes. Epilepsia 2016;57:1426–35.
Le Van Quyen M, Khalilov I, Ben-Ari Y. The dark side of high-frequency oscillations in the developing brain. Trends Neurosci 2006;29:419–27.
Lerner JT, Salamon N, Hauptman JS, Velasco TR, Hemb M, Wu JY, et al. Assessment and surgical outcomes for mild type I and severe type II cortical dysplasia: a critical review and the UCLA experience. Epilepsia 2009;50:1310–35.
Liu Z, Hu W, Sun Z, Wang X, Liu L, Shao X, et al. MRI abnormalities predominate in the bottom part of the sulcus with type II focal cortical dysplasia: a quantitative study. AJNR Am J Neuroradiol 2019;40:184–90.
McGonigal A, Bartolomei F, Regis J, Guye M, Gavaret M, Trebuchon-Da Fonseca A, et al. Stereoelectroencephalography in presurgical assessment of MRI-negative epilepsy. Brain 2007;130:3169–83.
Perucca P, Dubeau F, Gotman J. Intracranial electroencephalographic seizure-onset patterns: effect of underlying pathology. Brain 2014;137:183–96.
Roehri N, Pizzo F, Lagarde S, Lambert I, Nica A, McGonigal A, et al. High-frequency oscillations are not better biomarkers of epileptogenic tissues than spikes. Ann Neurol 2018;83:84–97.
Rosenow F, Luders H. Presurgical evaluation of epilepsy. Brain 2001;124:1683–700.
Talairach J, Bancaud J, Bonis A, Szikla G, Trottier S, Vignal JP, et al. Surgical therapy for frontal epilepsies. Adv Neurol 1992;57:707–32.
Tassi L, Colombo N, Garbelli R, Francione S, Lo Russo G, Mai R, et al. Focal cortical dysplasia: neuropathological subtypes, EEG, neuroimaging and surgical outcome. Brain 2002;125:1719–32.
Tassi L, Garbelli R, Colombo N, Bramerio M, Russo GL, Mai R, et al. Electroclinical, MRI and surgical outcomes in 100 epileptic patients with type II FCD. Epileptic Disord 2012;14:257–66.
Taylor DC, Falconer MA, Bruton CJ, Corsellis JA. Focal dysplasia of the cerebral cortex in epilepsy. J Neurol Neurosurg Psychiatr 1971;34:369–87.
Urbach H, Scheffler B, Heinrichsmeier T, von Oertzen J, Kral T, Wellmer J, et al. Focal cortical dysplasia of Taylor's balloon cell type: a clinicopathological entity with characteristic neuroimaging and histopathological features, and favorable postsurgical outcome. Epilepsia 2002;43:33–40.
Wagner J, Weber B, Urbach H, Elger CE, Huppertz HJ. Morphometric MRI analysis improves detection of focal cortical dysplasia type II. Brain 2011;134:2844–54.
Wang ZI, Jones SE, Jaisani Z, Najm IM, Prayson RA, Burgess RC, et al. Voxel-based morphometric magnetic resonance imaging (MRI) postprocessing in MRI-negative epilepsies. Ann Neurol 2015;77:1060–75.
Worrell G, Gotman J. High-frequency oscillations and other electrophysiological biomarkers of epilepsy: clinical studies. Biomark Med 2011;5:557–66.